



HAL
open science

Plasmon resonance measurements in pool boiling, condensation and evaporation experiments.

Frédéric Lefèvre, Mostafa Al Masri, Joyce Ibrahim, Colette Veillas, Isabelle Verrier, Frédéric Celle, Olivier Parriaux, Yves Jourlin, Serge Cioulachtjian

► To cite this version:

Frédéric Lefèvre, Mostafa Al Masri, Joyce Ibrahim, Colette Veillas, Isabelle Verrier, et al.. Plasmon resonance measurements in pool boiling, condensation and evaporation experiments.. International Journal of Heat and Mass Transfer, 2022, 184, pp.122286. 10.1016/j.ijheatmasstransfer.2021.122286 . hal-03522949

HAL Id: hal-03522949

<https://hal.science/hal-03522949>

Submitted on 19 Jan 2022

HAL is a multi-disciplinary open access archive for the deposit and dissemination of scientific research documents, whether they are published or not. The documents may come from teaching and research institutions in France or abroad, or from public or private research centers.

L'archive ouverte pluridisciplinaire **HAL**, est destinée au dépôt et à la diffusion de documents scientifiques de niveau recherche, publiés ou non, émanant des établissements d'enseignement et de recherche français ou étrangers, des laboratoires publics ou privés.

Plasmon resonance measurements in pool boiling, condensation and evaporation experiments

F. Lefèvre¹, M. Al Masri¹, J. Ibrahim², C. Veillas², I. Verrier², F. Celle², O. Parriaux², Y. Jourlin², S. Cioulachtjian¹

¹ Univ Lyon, CNRS, INSA-LYON, CETHIL UMR5008, F-69621 Villeurbanne, France

²Laboratoire Hubert Curien UMR CNRS 5516, Univ. of Lyon, 42000 Saint-Étienne, France

ABSTRACT

The surface plasmon resonance (SPR) method, using a periodic corrugated surface, is implemented on aluminium samples on which different liquid-vapour phase change phenomena take place. The objective is to study the plasmonic response in the presence of these phenomena, and in particular to evaluate the capacity of the plasmonic method to provide information at the sub-micron scale, which is still little explored in phase change experiments. The first part of the paper presents experimental results of pool boiling obtained on mirror-polished surfaces with different geometrical patterns (holes and pillars periodically patterned as 1D gratings). The results show that the heat transfer characteristics of the surface are improved with a small number of holes evenly distributed over the surface. The samples covered with 1D gratings are then used in the last part of the paper to implement the SPR method and analyse measurements obtained in pool boiling, condensation and evaporation. The optical method based on SPR was not able to detect the birth of the first vapour nuclei at the onset of nucleate boiling due to the very fast growth of the bubbles. However, the results show the interest of the method as a non-intrusive technique for measuring the temperature of the liquid in the very vicinity of the wall. Moreover, measurements in condensation and evaporation experiments usefully monitor in real time the formation of a nanoscale condensation film and the evaporation of an acetone film.

Keywords Boiling, Evaporation, Condensation, Ultra-smooth surfaces, Surface Plasmon Resonance, Nucleation

1. INTRODUCTION

It has been assessed both experimentally and theoretically that the nature of the solid surface and its structuring even at a sub-micron scale strongly affect the phase change heat transfer characteristics (boiling, evaporation, condensation, freezing) because it changes the interfacial structure and the activities of fluid molecules adjacent to the solid surface. Analysis of physical phenomena during phase change therefore requires the development or adaptation of innovative techniques capable of exploring phenomena at this little-explored scale.

The emergence of micro and nanotechnologies has made it possible to control the texture and chemistry of surfaces at high resolution on scales ranging from the molecule to the centimetre, paving the way for improving the efficiency of phase change phenomena [1][2]. Improving the efficiency of liquid-vapour phase change also requires the development of models and correlations, validated by accurate measurements of wall temperatures and liquid-vapour flow parameters, which are usually obtained by optical methods [3][4]. By their nature, these experimental methods are limited in minimum size by the wavelength of the light. However, it may be necessary to understand phenomena developing at smaller scales, such as the study of nucleation in the case of boiling [5], condensation [6] and freezing [7], or the study of interfacial phenomena occurring at the liquid-vapor interface [8] or at the triple line [9].

Methods based on surface plasmons (SP) enable measurements down to sub-micron scales and are therefore promising to achieve this goal.

Surface plasmons are a collective oscillation of free electrons on the surface of a metal in contact with a dielectric medium under the effect of a high frequency electromagnetic excitation, such as visible light under transverse-magnetic (TM) polarization [10]. In this interaction, the free electrons oscillate in resonance with the incident light wave, absorbing the photons of the incident light at the resonance frequency. As a result, the intensity of the light reflected at the metal/dielectric interface is reduced at the wavelength of the surface plasmon resonance (SPR). The resonance frequency depends on the properties of the metal but also of the dielectric medium. Therefore, any change within the dielectric in the vicinity of the metal/dielectric interface would modify the SPR wavelength, offering the possibility to develop a non-intrusive optical sensor to detect this modification. The SPR mode propagates along the interface of a metal/dielectric interface, but decays very rapidly perpendicularly to the surface and is therefore qualified of evanescent wave. The skin thickness in the dielectric, which is the thickness for which the amplitudes of the electric and magnetic field are attenuated perpendicular to the surface is of the order of half the wavelength of the light involved [10], paving the way to the development of subwavelength optical sensors [11]. Therefore, SPR are of interest to a wide range of applications including biology, physics or material science. However, to our knowledge, the applications in the field of phase change heat transfer are very recent.

Historically, surface plasmons were first considered by Sommerfeld in 1899 [12] and then by Zenneck in 1907 [13], and the first observation of surface plasmons by Robert W. Wood in 1902 was made during reflectivity measurements on metal gratings [13]. Since then, research on SP and their applications has developed strongly. As early as the 1970s, they were used for the characterization of thin films [15] and for spectroscopy [16]. The high sensitivity of surface plasmons to the structure of interfaces enables them to be used as chemical [17] [18] and biological sensors [19] [20] [21]. SP are exploited in many other devices, where they play an intermediary role to improve their performance, such as photovoltaic cells [22] [23]. Being very sensitive to the external environment, SP are exploited in refractometry. The short propagation length of surface plasmons has made it possible to realize nano-emitters [24] and very small circuits [25]. The work of Sauvage-Vincent [26] focused on resonant plasmonic transmission applied to an optical security component. From a fundamental point of view, plasmonic has made it possible to study the behaviour of light at the nanoscale. The intense activity concerning plasmonic has been made possible by the development of nanofabrication techniques [27] and near-field microscopy techniques [28].

Recently, Jeong et al. [29] [30] presented experimental measurements of nanoscale thin frost layers by SPR; the authors were able to visualize the submicron frost layers between frozen droplets and reported the quantitative evolution of frost layer thickness. At about the same time, Ibrahim et al. [31] show that SPR could be used to detect the condensation of acetone vapor on an aluminium plate cooled down in a two-phase environment and in a following paper [32] that SPR could be used as a non-invasive, high-resolution temperature measurement method for metallic surfaces. Even more recently, following the papers of Jeong et al. of [29] [30], Kim et al. [33] applied SPR to the measurements of the profiles that cover part of the evaporating thin film and the adsorbed film in the contact line region. The two teams involved in these works related to phase change phenomena used two different optical devices to excite the SP: the first a prism [29] [30] [33], and the second a grating [29] [30].

The classical mathematical formalism describing surface plasmons is based on Maxwell's equations. Surface plasmons are magnetic transverse polarized modes of vibration, i.e. the evanescent magnetic field associated with these plasmons is normal to the plane of incidence.

Therefore, on a flat metallic surface, it is not possible to excite surface plasmon modes and thus, SPR do not absorb the incident photons. There are three main techniques to excite the surface plasmon [10]. The most commonly employed approach is based on the attenuated total reflection method in a prism-based structure. The second technique relies on a topological defect to cause scattering and enables to create a localized surface plasmon in the vicinity of this defect. This phenomenon is at the origin of the very particular optical properties of the Lycurgus Cup, manufactured during the roman era, which colour turns from green to red when it is illuminated [34]. In the third technique, which is used in the results presented in this paper, a periodic corrugation in the surface of the metal, such as a 1D grating, enables to couple the surface plasmon to the light.

Homola et al. [35] showed that in angular interrogation mode, the sensitivity of SPR sensors using diffraction gratings does not differ significantly from that of SPR sensors based on prism couplers. However, the implementation of these two techniques is different. In the first method using a prism, light is transmitted through the prism and reflected from the back of a metal plate in contact with a prism, with the dielectric at the front. Therefore, light does not pass through the dielectric fluid. In the grating method, the excitation light and its reflection must pass through the dielectric material. This is a major drawback of this method. However, in most phase change experiments, the surface under study must be cooled or heated on the back side, which makes it difficult to fix a prism on the back side. This disadvantage is not found with the SPR method using a corrugated surface to excite the SPR mode.

In this paper, we present results obtained with the SPR method on a corrugated surface in different liquid-vapour phase change experiments. First, the SPR method is used in a pool boiling rig, to see if this method can shed new light on understanding the mechanisms of bubble incipience. In order to interpret these results, the grating-coated aluminium samples are first tested in a pool boiling rig in order to plot their boiling curve and estimate their thermal performance. As the gratings are realized on a mirror-polished surface, this part of the paper completes a previous study by Al Masri et al. [2] on nucleated boiling on ultra-smooth surfaces. After a brief review of the previous results [2], we present, in addition to the results obtained with the gratings, new experimental results on an ultra-smooth surface where a few holes were evenly machined on the surface using a femtosecond laser. In the last part of the paper, we analyse experimental results obtained in evaporation and condensation, completing the preliminary results and analyses presented in [31].

2. DESCRIPTION OF THE SAMPLES MADE FOR THE STUDY OF BOILING AND CONDENSATION BY SURFACE PLASMON RESONANCE

As it was explained in the introduction, there are different possibilities to produce surface plasmon resonance on a surface in contact with a fluid: diffraction at gratings or attenuated total reflection in prism couplers. In this work, diffraction at gratings under spectral interrogation (Figure 1) was chosen to study different phase change phenomena at the interface between a heated or a cooled surface and a liquid in equilibrium with its vapor.

When a TM polarized collimated white light is incident at a fixed angle on a metallic grating, the intensity of its reflection is selectively reduced according to the wavelength, with an absorption peak corresponding to the resonance and that is related to the excitation of the polariton plasmon. The resonance wavelength depends on the refractive index of the fluid, which is very close to 1 for the vapor phase, whatever the working fluid, and is always larger for the liquid phase and depends on its temperature. Therefore, by analysing the intensity

variation of the reflected wavelengths, it is possible to discriminate the gas phase from the liquid phase at a scale of a few nanometres in the fluid in a direction perpendicular to the solid surface.

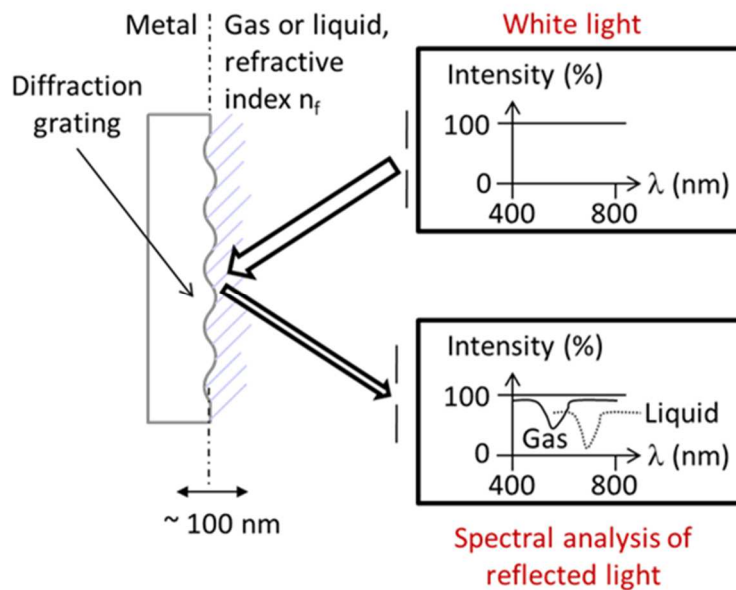


Figure 1: Reflectance of collimated TM polarized white light on a metallic grating due to Surface Plasmon Resonance

The implementation of the gratings on the study area is realized by laser interference photolithography (grating characteristics are described further), on a mirror-polished surface. In a previous study described in the introduction [2], we used aluminium samples to study the influence of the roughness on nucleate boiling on ultra-smooth surfaces. These samples are therefore well suited to implement the surface gratings required for the present study.

Figure 2 (a) presents a cross section of this sample, which is basically a thin aluminium cylinder of height 5 mm and diameter 80 mm. The area of interest for the study of nucleate boiling or condensation is a circle with a diameter of 25 mm located in the middle of the upper face of the sample. This configuration, with a large sample diameter compared to the area of interest was chosen to prevent the formation of parasitic bubbles at the periphery of the studied area. Indeed, as the initial objective was to detect the formation of the first bubble on the surface, the surface was designed to avoid the formation of spurious bubbles. In conventional devices, the first bubbles always nucleate at the periphery of the surface. Nucleation is promoted in the gaps between the test surface and the other parts of the experimental bench or by the non-wettability of the liquid on the hot insulating substrate in contact with the test surface, or possibly on the adhesive applied to fill the gaps. These parasitic bubbles promote the propagation of boiling on the surface. Therefore, the onset of nucleate boiling (ONB) and the wall superheating at the beginning of boiling can be severely impacted. To avoid the formation of these first bubbles, the surface should not show any discontinuity between the area of interest and its periphery.

On the bottom face of the sample, a cylindrical groove of width $w_g = 5$ or 10 mm was realized in order to reduce heat loss to the periphery of the sample. Despite this groove, the thickness of the remaining fin between the surface of interest and the periphery of the system remains significant for mechanical reasons (~ 0.2 mm) and a numerical model was developed to estimate the actual flux transferred into the area of interest. On the bottom of the area of interest, a thin heater, a thermocouple and a fluxmeter enable to measure the temperature and the heat flux

entering the sample. The entire surface is first mirror polished and then, on the area of interest, artificial microsities can be machined to modify the two-phase heat transfer characteristics. More details concerning the model and the experimental procedure can be found in the paper of Al Masri et al. [2].

Figure 2 (b) and (c) presents pictures of the upper face of the raw sample and the mirror-polished sample respectively. In some mirror-polished samples, a few holes were machined using a femtosecond laser to complete the investigation presented in [2]. Figure 2 (d) presents the topography of one of these holes measured by confocal microscopy. Diameters and heights in the range 7 - 20 μm and 7 - 30 μm were measured respectively.

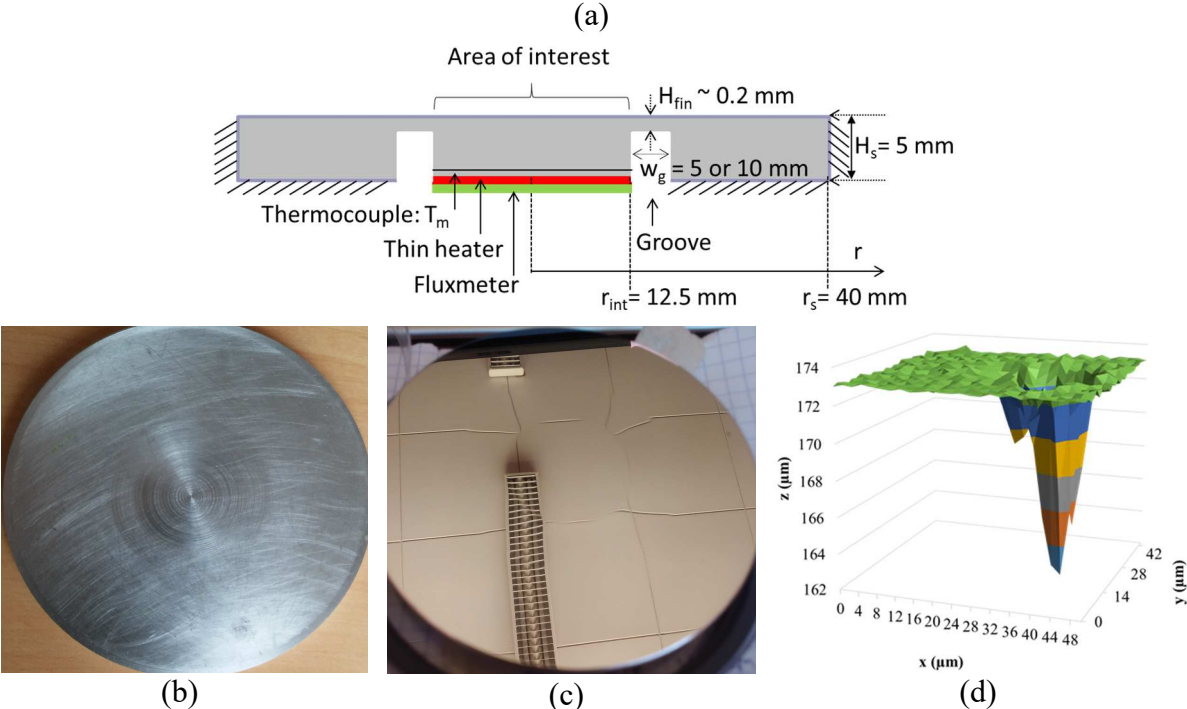


Figure 2: Aluminium sample for pool boiling and condensation experiments; (a) cross-section of the sample; (b) raw sample; (c) mirror-polished sample; (d) characterization of a hole on a mirror-polished sample

Figure 3 presents the mirror-polished aluminium sample on which the diffraction grating was etched following the procedure described in Ibrahim et al. [31].

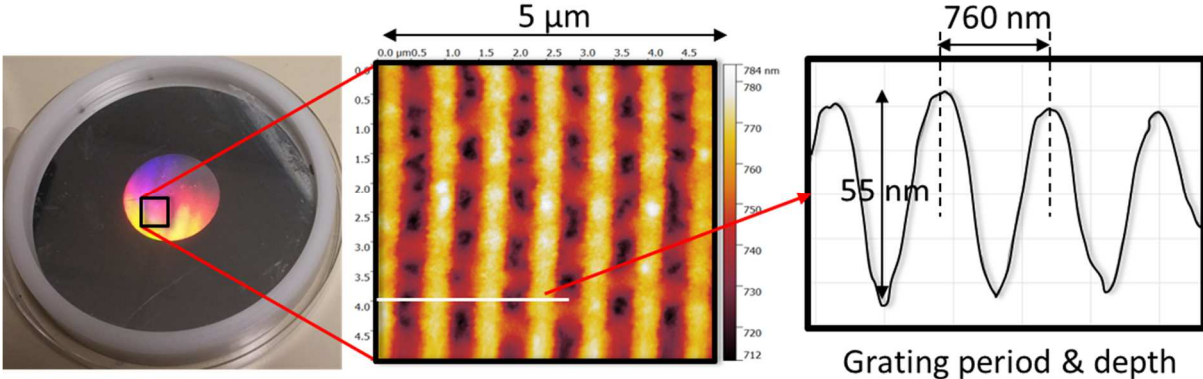


Figure 3: Diffraction grating ($D = 25 \text{ mm}$) and AFM topography measurements

The grating covers the entire area of interest and has a sinusoidal shape of depth 55 nm and period 760 nm. These dimensions were chosen numerically to implement the plasmonic resonance measurements with the best resolution (greatest amplitude of reflection) under the conditions of the experiment. Further details regarding the design and the etching process of these surfaces can be found in the papers [31] and [32].

3. POOL BOILING MEASUREMENTS

This section presents pool boiling curves obtained with the samples presented in section 2. The influence of different surface finishes on the boiling phenomena are assessed, including the surface with the diffraction grating used in section 4 for plasmon resonance measurements. Some experimental results were already presented in [2], which led to the development of a new surface finishes, the results of which are also presented in this section.

3.1. Pool boiling experimental rig

The experimental rig for pool boiling experiments is shown in Figure 4.

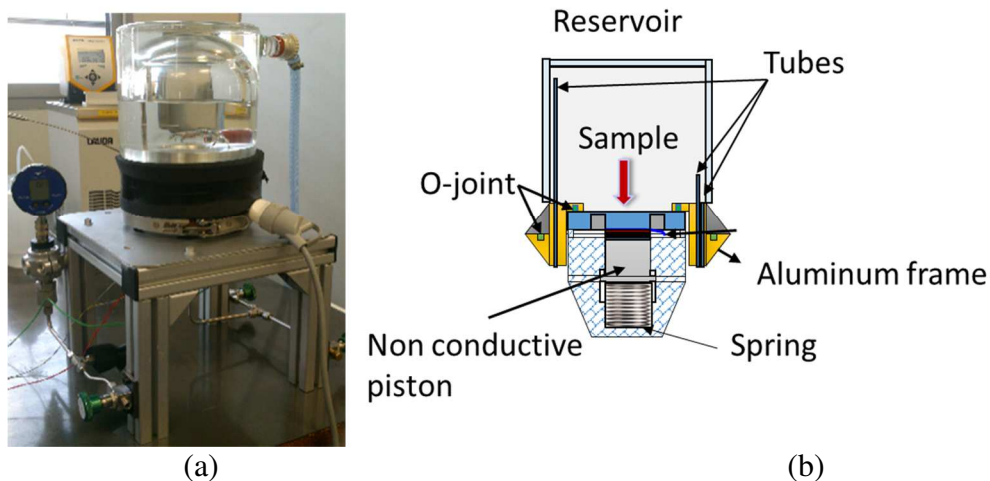


Figure 4: Pool boiling experimental bench; (a) picture of the experimental rig; (b) schematic of the transparent reservoir with the sample

A transparent reservoir with a double wall is connected to a thermostatic bath in order to control the saturation temperature inside the reservoir. The transparent container is hermetically sealed to an aluminium holder with a PTFE O-ring and clamp, allowing the system to be opened and the test sample easily changed. The aluminium sample is tightly packed against the aluminium holder. Therefore, the pool boiling experiment is fully hermetically sealed with two O-rings. Several tubes are used to empty and fill the system, but also to insert thermocouples within the reservoir in order to measure the saturation temperature. Acetone was used as the working fluid for its compatibility with aluminium. During the experiments, the saturation temperature of the reservoir was maintained at 56 °C, which corresponds to a pressure of 1 bar. More details on this experimental bench are provided in [2].

3.2. Pool boiling experimental results

Figure 5 presents typical boiling curves obtained by Al Masri et al. [2] with three different surface finishes, whose root mean square (RMS) is measured by confocal microscopy : an unpolished raw surface (b), a mirror-polished surface (c), a mirror-polished surface with a few unintended defects, that were observed and described by confocal microscopy (d). Defects are surface holes with a depth greater than 20 μm . A detailed description of these surfaces is presented in [2]. The boiling curves are plotted using the heat flux Q , which is dissipated above the area of interest and the temperature difference between the temperature measured at the middle of the sample T_m and the saturation temperature T_{sat} .

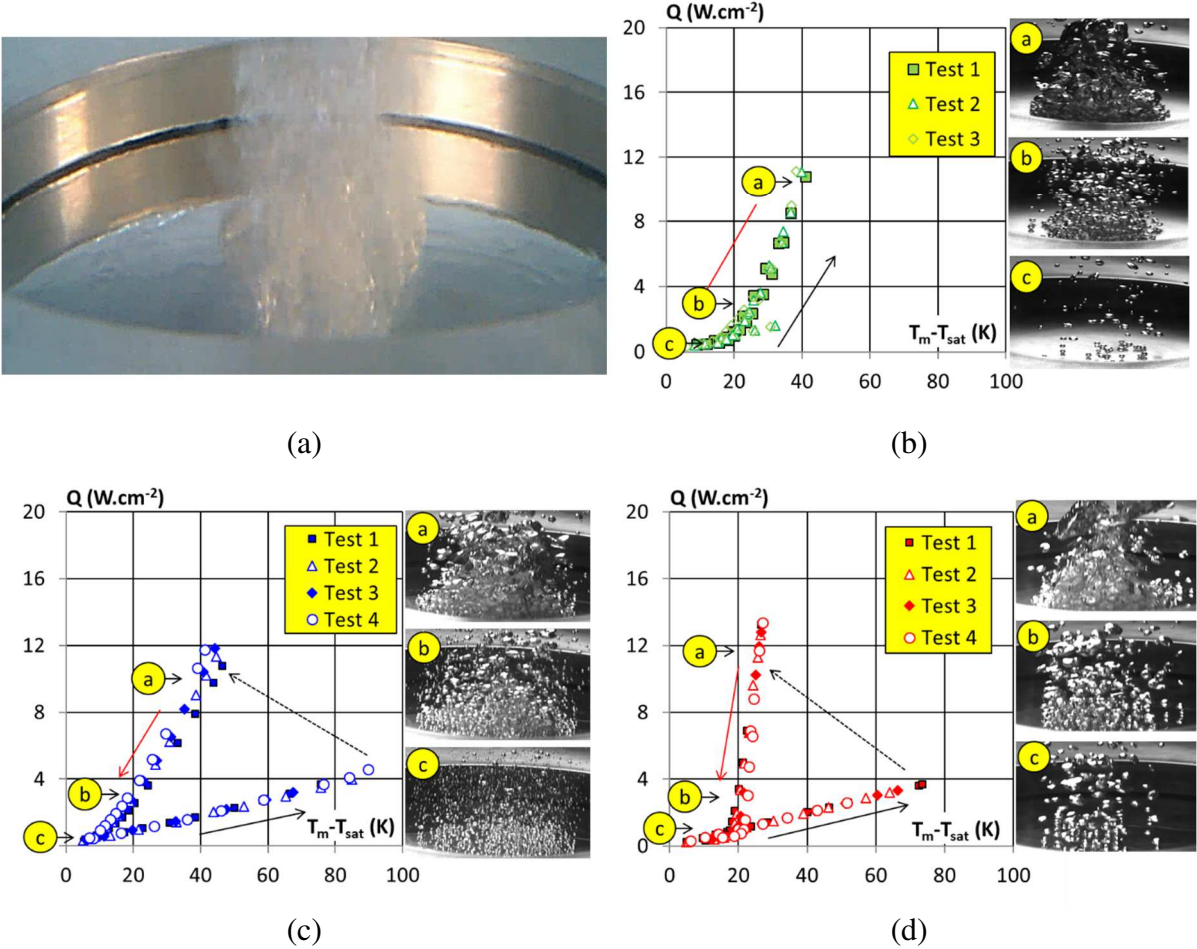


Figure 5: Typical boiling curves obtained by Al Masri et al. [2]; (a) nucleate boiling on the area of interest; (b) unpolished raw surface (RMS = 5200 nm); (c) mirror-polished surface (RMS = 60 nm); (d), mirror-polished surface with 10 unintended defects (characteristic length:5 to 25 μm)

Figure 5 (a) shows that nucleate boiling occurs only over the area of interest, with the circular groove at the bottom of the sample limiting the heat diffusion to the sample periphery, as explained in the previous section. However, for increasing heat flux, during the natural convection phase, the heat flux tends to be distributed over the entire surface of the sample due to the very low convection heat transfer coefficient. After the ONB, the heat flux mainly flows in the central area of interest where nucleate boiling occurs. The numerical model was used to estimate the surface density flux in the area of interest. This explains why Q suddenly increases from 4 $\text{W}\cdot\text{cm}^{-2}$ to 12 $\text{W}\cdot\text{cm}^{-2}$ at the ONB for the same power supplied by the heater (dotted arrow in the curves of figures 5). In these experiments, in order to preserve the resistor, the power supplied to the resistor was just limited to that required to initiate boiling. Thus, the

boiling curve is limited to $Q = 12 \text{ W/cm}^2$. Therefore, the critical heat flux was never reached in these conditions.

For each experiment, several tests were realized for increasing and decreasing heat fluxes to assess the repeatability. Three pictures of the area of interest are presented for decreasing heat fluxes. The major conclusions of this work [2] were the following:

- **Unpolished raw surface:** a small superheat is required for boiling incipience, which is progressive and occurs when the temperature difference between the sample and the saturation temperature reaches 30 K. The hysteresis between increasing and decreasing curves is small. At low decreasing heat flux, a limited number of nucleation sites survive at some locations on the surface.
- **Mirror-polished surface with no defects:** a huge superheat is required to start boiling. For increasing heat flux, natural convection occurs as long as the temperature difference between the sample and the saturation temperature is below 90 K, at which point explosive boiling occurs by reducing the temperature difference to 30 K for the same heat flux. There is a very large ONB hysteresis between increasing and decreasing curves with the presence of a huge number of very small bubbles surviving at very low decreasing heat flux for a temperature superheat lower than 10 K.
- **Mirror-polished surface with a few defects:** an important superheat is required to start boiling. As with the same surface without defects, boiling incipience is explosive, with a large hysteresis but lower than that of the unpolished surface. At low decreasing heat flux, a limited number of nucleation sites survive at some locations over the surface until the system returns to natural convection for a temperature superheat of about 20 K.

When comparing the decreasing heat curves for the three samples, one can see that for the same heat flux dissipated over the area of interest, the temperature superheat ($T_m - T_{sat}$) is lower for the mirror-polished surface with a few defects, leading to a better thermal exchange during nucleate boiling. Al Masri et al. [2] explained that these defects act as point heat sinks, concentrating the heat flux lines coming from the heater. These defects being separated by an ultra-smooth area, no parasitic bubbles are to be found around these spots and therefore, the coalescence process is postponed, leading to a small increase of the superheat when the heat flux increases.

Based on the conclusions of this paper, a new sample was created with 24 holes evenly distributed over the entire area of interest, as described in the previous section. The boiling curve produced with this new sample as well as the boiling curve obtained with the sample covered with the gratings are presented in Figure 6 (a) and (b) respectively.

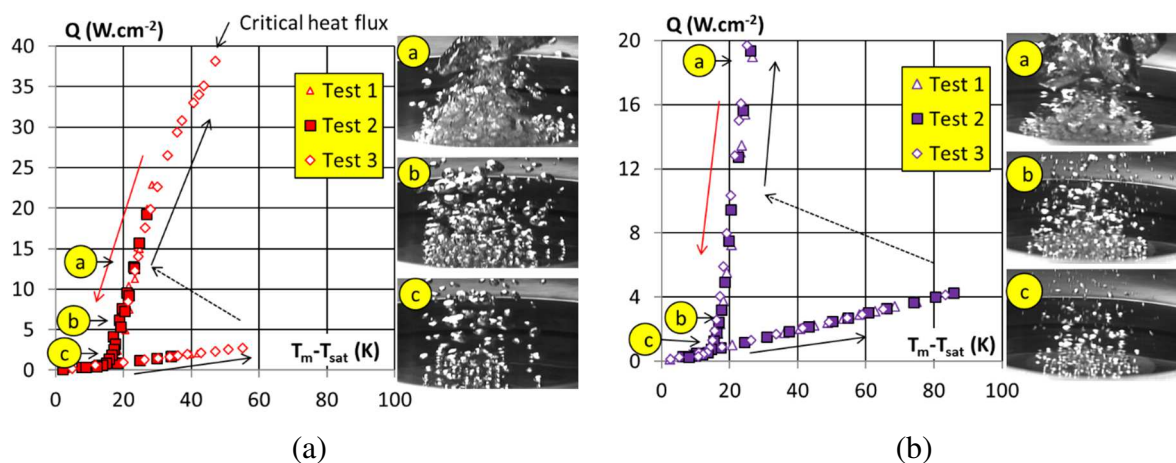


Figure 6: Boiling curves; (a) mirror-polished surface with 24 holes; (b) mirror-polished surface with grating

For the first sample, presented in Figure 6 (a), a complete boiling curve was plotted for one single test until the critical heat flux was reached at a high value of about 40 W.cm^{-2} . The findings of this new test confirm those obtained with the sample with unintended defects, with even better thermal performance due to a higher number of holes well distributed over the surface. This confirms the benefit of developing a polished surface with well distributed holes to improve the boiling thermal performance of a surface. Further tests could be carried out with an even larger number of holes to study both the improvement of the heat transfer coefficient and the influence on the critical heat flux.

The boiling curve for the surface covered with the gratings (Figure 6 (b)) is very similar to that in Figure 6 (a). A huge superheat of about 90 K is required to start boiling as for the mirror-polished surface. There is an incomplete hysteresis between increasing and decreasing curves with a superheat even smaller than that of the mirror-polished surface with 24 holes. This behaviour is difficult to explain because the depth of the grating is very small (50 nm) compared to its period (760 nm). It is possible that the surface treatment used to form the network modifies the wettability of the surface, but this hypothesis remains to be confirmed.

Figure 7 presents a synthesis of the different boiling curves, showing that ultra-smooth surface with holes and the surface with gratings requires a huge superheat for the incipience of boiling, but have the lower superheat for a given heat flux when boiling has started. Further investigations are needed to improve the understanding of these results, for example by increasing the number and the characteristic length of the holes and by changing the depth and the period of the gratings. However, the actual characteristics of the surface with the gratings were chosen to get the best resolution for the plasmon resonance measurements, which are presented in the next section. One of the aspects we wanted to investigate with this measurement technique is the possibility of measuring the birth of the first vapor nuclei at the incipience of boiling.

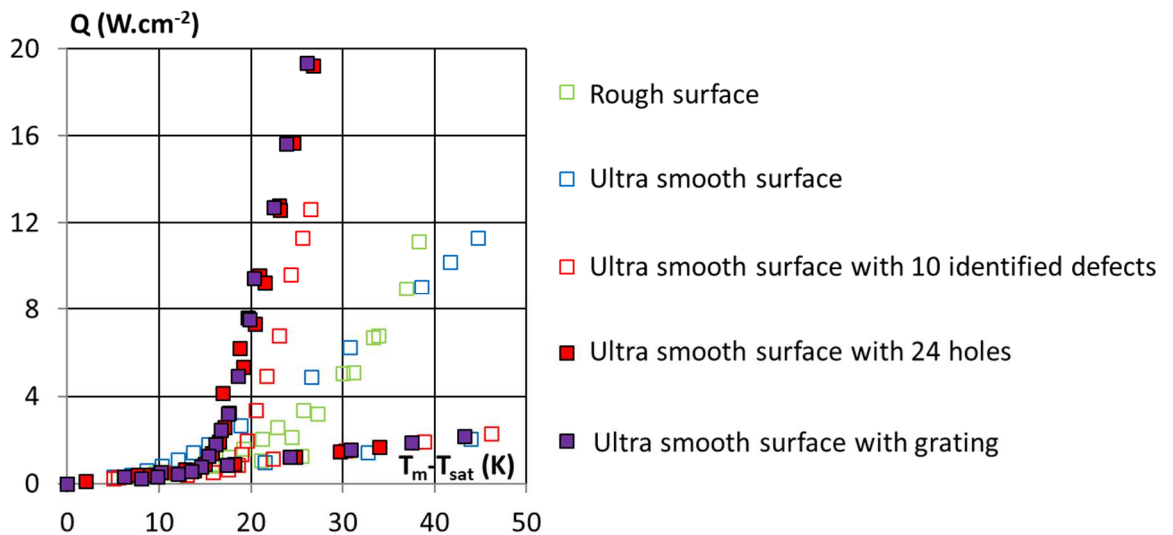


Figure 7: Synthesis of the boiling curves plotted for the different samples studied in this work

4. PLASMON RESONANCE MEASUREMENTS IN POOL BOILING AND CONDENSATION EXPERIMENTS

4.1. Plasmon resonance experimental bench

A new experimental bench was built to implement the plasmon resonance optical equipment into a pool boiling experiment. In particular, the transparent part of the tank must be flat and of good optical quality to enable the measurement to be carried out. Furthermore, to facilitate the optical measurement, the sample is positioned vertically rather than horizontally. Figure 8 presents a schematic of this bench. A flat glass window is hermetically sealed to an aluminium holder with a PTFE O-ring and clamp, allowing the system to be opened and the test sample easily changed. The aluminium sample is tightly packed against the aluminium holder. Contrary to the experimental rig presented in the previous section, the saturation temperature of the pool is controlled by several heaters inserted within the aluminium holder or plated against it. The energy from these heaters is used to compensate for heat loss by natural convection and radiation through the glass wall. This maintains the temperature of the reservoir at the user's target saturation temperature. Heat flux and temperature measurements for the boiling curve are carried out following the same procedure as the experiment in Section 3.

Figure 9 (b) presents a picture of the reservoir where nucleate boiling on the area of interest can be observed. A third reservoir was realized for this experiment, which is shown in Figure 9 (a). Unlike the previous two reservoirs, which were designed to withstand a maximum saturation pressure of 2 bar, this third tank can withstand a pressure of up to 20 bar. The purpose of this third tank is to calibrate the measurement obtained by the optical system, following a procedure explained in section 4.2. Figure 9 (c) shows the optical equipment composed of a halogen source, a polarizer and a spectrometer. The source and the spectrometer are connected to optical fibres and light is collimated by lenses just in front of each fibre. The location of these devices in relation to the pool boiling test rig are visible in Figure 9 (b).

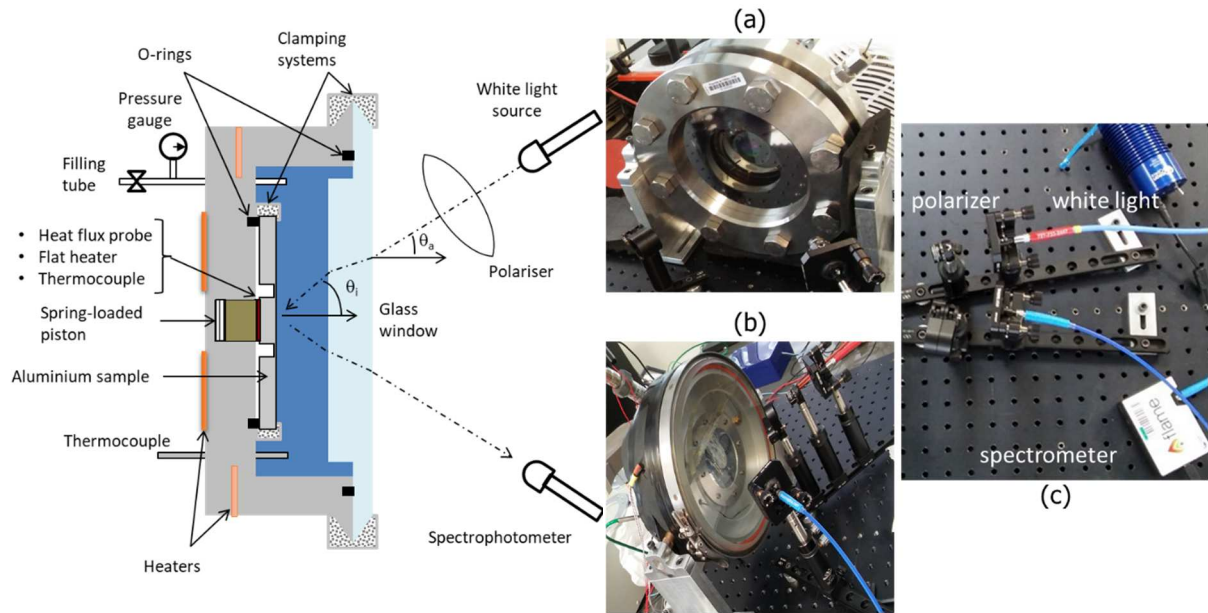


Figure 8: Pool boiling experimental bench for plasmon resonance measurements implementation

Figure 9: Pictures of the experimental rigs; (a) calibration bench; (b) pool boiling setup; (c) optical equipment for plasmon resonance measurements

4.2. Calibration of the SPR in two-phase conditions

The wavelength of resonance λ_{SPR} depends on several parameters, which are linked by the following expression: $\lambda_{SPR} = n_{SPR} \cdot \Lambda \cdot (1 - \sin\theta_i)$ where n_{SPR} is the index of refraction of the fluid for the resonance wavelength λ_{SPR} and at the temperature T just above the gratings, Λ the period of the grating and θ_i the angle of incidence of the white light on the grating (Figure 8).

Therefore, the value of λ_{SPR} is directly related to the very local index of refraction of the fluid just above the grating. Because white light passes through a glass plate with parallel faces (Figure 8), the value of θ_i depends only on $n(\lambda, T)$, on the angle θ_a between the white light and the glass and on the index of refraction of air n_a through the following relation: $n(\lambda, T) \sin\theta_i = n_a \sin\theta_a$. During the experiments, the value of the angle θ_a was estimated with an accuracy of $\pm 2^\circ$. The value of n_a being very close to 1, the wavelength of resonance can therefore be expressed:

$$\lambda_{SPR} \cong \Lambda \cdot (n(\lambda, T) - \sin\theta_a) \quad (1)$$

Figure 10 presents an example of measurements of the reflected light on the grating in contact with acetone vapor. The surface plasmon resonance (SPR) is clearly visible at a wavelength of about 550 nm, where the reflectance is lower due to the absorption of light by the surface plasmon. The angle θ_a was estimated to 15° in this experiment. Given the period of the grating $\Lambda=760$ nm, and $n(\lambda, T) \sim 1$ for the vapour regardless of λ and T , the calculated wavelength of resonance is equal to 550 nm, which is consistent with the experimental measurements. When the grating is in contact with liquid, the value of the index of refraction depends on both the wavelength and the temperature of the liquid in the vicinity of the gratings. The wavelength dependence of the refractive index can be evaluated using the Cauchy dispersion formula [36]: $n(\lambda) = A+B \cdot \lambda^{-2} + C \cdot \lambda^{-4}$ with $A = 1.34979$ (at $T = 20^\circ\text{C}$), $B = 0.00306$ and $C = 0.00006$ for acetone and λ in μm . A linear variation of the refractive index of acetone with temperature was determined in [37] $n(T) = n(0^\circ\text{C}) - 0.00050747T$ for

$0\text{ }^{\circ}\text{C} < T < 60\text{ }^{\circ}\text{C}$. Combining these two expressions leads to the following expression for the index of refraction of acetone:

$$n(\lambda, T) = (1.34979 - 0.00050747(T-20) + 0.00306\lambda^{-2} + 0.00006\lambda^{-4}) \quad (2)$$

The calibration reservoir (Figure 9 (a)) is used to calibrate the detector response as a function of the saturation temperature. In contrast to the other experimental rig ((Figure 9 (b)) in which the reservoir temperature is fixed at $T_{\text{sat}} = 56\text{ }^{\circ}\text{C}$ while the sample is heated to plot the boiling curve, in the third reservoir, the saturation temperature of the reservoir itself is changed between $10\text{ }^{\circ}\text{C}$ and $120\text{ }^{\circ}\text{C}$, with the sample fully immersed in the tank. For this reason, the reservoir has to sustain the huge saturation pressure reached for high temperature of acetone. This experience makes it possible to plot the SPR wavelength measurements versus the temperature of the reservoir and thus to calibrate the temperature response of the optical system.

Figure 11 presents the SPR wavelength versus increasing and decreasing reservoir temperatures for two different angles of incidence of the light on the glass slab ($\theta_a = 30^{\circ}$ or $\theta_a = 35^{\circ}$). By integrating equation (2) in equation (1), λ_{SPR} can be calculated knowing the angle θ_a . As the uncertainty on θ_a is important in our experiment, the two values of θ_a are fitted by comparison with the experimental data. A good concordance is found between the experimental and calculated wavelength of resonance (dotted lines) for two fitting angles in the range of the experimental uncertainty ($\theta_a = 28.2^{\circ}$ or $\theta_a = 34.1^{\circ}$). For temperatures above $100\text{ }^{\circ}\text{C}$, the experimental data tend to deviate from the theoretical curve, which is probably due to the variation of the refractive index with temperature which can no longer be considered linear in this range. It is possible to take this variation into account by including an additional polynomial term of degree 2 in the refractive index. The factor in front of this term is also estimated by comparison with the experimental data (solid line in Figure 11) leading to the following expression for $n(\lambda, T)$:

$$n(\lambda, T) = (1.34979 - 5.0747 \times 10^{-4}(T-20) - 3.622 \times 10^{-7}(T-20)^2 + 0.00306\lambda^{-2} + 0.00006\lambda^{-4}) \quad (3)$$

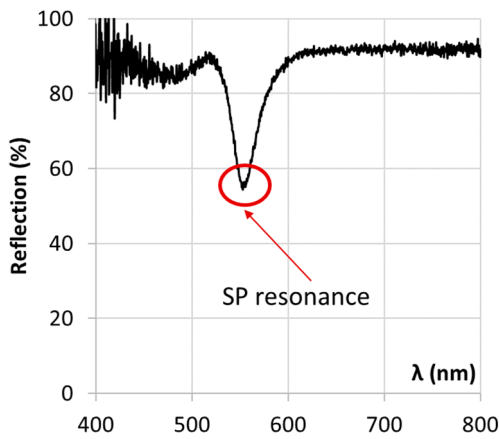


Figure 10: Example of SP resonance measured by reflection of white light on the grating in contact with vapor, $\theta_a = 15^{\circ}$

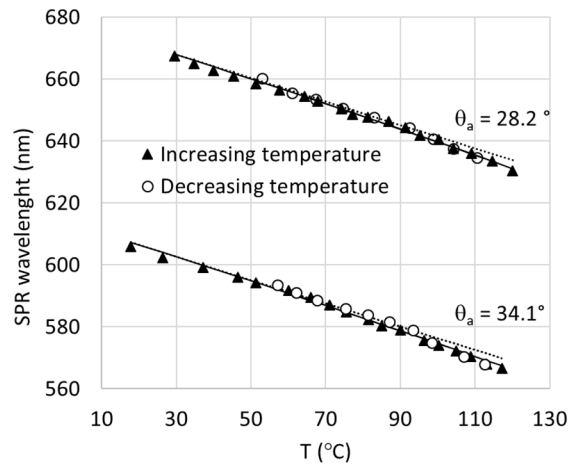


Figure 11: SPR wavelength in the liquid phase versus T_{sat} for two different incidence angles; dotted line plotted with Eq. 2 and solid line with Eq. 3

4.3. Plasmon resonance measurements to detect the boiling incipience

The SPR optical equipment was implemented in the pool boiling set-up (Figure 9 (b)). Figure 12 presents the evolution of the SPR for increasing heat flux imposed on the sample in contact with the liquid phase, the saturation temperature being equal to 56 °C (1 bar). For each step of heat flux, SPR is recorded when the thermal equilibrium is reached. The plasmon resonance measurements was recorded for increasing heat flux. Contrary to the boiling curve presented in Figure 6 (b), where the power is increased in relatively large steps of about 0.3 W.cm⁻², for this experiment, the steps of heat flux are about 6 times lower, in the hope of detecting a change in the plasmonic signal and of following the formation of the nucleation at its site. A linear decrease is observed with increasing wall temperature at the middle of the sample. At the ONB, the explosive nature of the incipience prevents to record any change of the SPR. The detector does not pick up the first moments of the growth of the bubbles because the bubble grows much faster [2] than the minimum integration time of the optical system which is about 1 ms. An ultra-fast spectrometer shall be used for this purpose. Then, once nucleate boiling has started, the presence of the bubbles prevents the measurements of any signal due to the multiple reflections and scattering of the light on the bubbles. Therefore, the method can only be used for the natural convection part of the boiling curve.

The measurements show a deviation of the SPR towards shorter wavelengths with increasing superheat. This evolution is due to the decrease of the refractive index of the medium when the temperature of the fluid increases. For a given angle of incidence, the calibration law (equation 3) is compared to the experimental data presented in Figure 12. This comparison is shown in Figure 13 for $\theta_a = 32.9^\circ$. The figure shows a good agreement between the temperature of the sample measured by the thermocouple and the temperature of the sample measured using the SPR calibration curve for an incident angle of 32.9°.

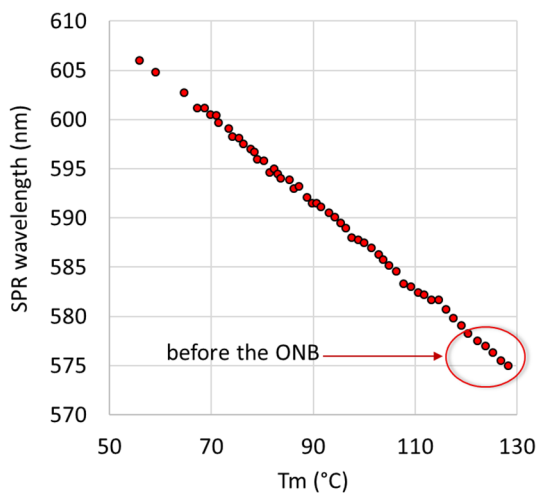


Figure 12: SPR wavelength for increasing heat flux at the aluminium/acetone interface, $T_{sat} = 56 \text{ }^\circ\text{C}$; $\theta_a = 35^\circ$

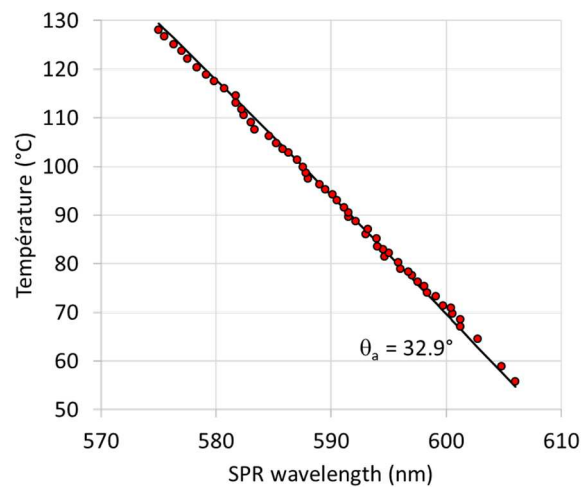


Figure 13: Comparison between the temperature of the sample measured by the thermocouple or by the SPR method using the calibration formula (Eq. 3)

To conclude this section, it can be said that the optical method based on SPR was not able to detect the birth of the first vapour nuclei at the ONB due to the very fast growth of the bubble. Moreover, the results show the interest of the method as a non-intrusive technique for measuring the temperature of the liquid in the very vicinity of the wall, which offers important perspectives for the study of many heat transfer phenomena such as natural or forced convection, as it was mentioned in [32]. In the next section, the surface plasmon method is

tested to detect the first moment of the condensation on a surface and the last moment of evaporation from a liquid film.

4.4. Plasmon resonance measurements in condensation and evaporation experiments

In order to evaluate the ability of the method to detect a change in the state of the fluid close to the grating, the second boiling test rig (Figure 9 (b)) was also used for condensation and evaporation tests. For these experiments, the reservoir is filled with a small amount of liquid, therefore the area of interest of the aluminium sample is in contact with vapour rather than liquid. As the sample and the experimental rig were not designed for condensation experiments, it is not possible to insert a cold source on face of the aluminium sample. The condensation experiment was carried out by heating the glass surface of the reservoir, which creates a small thermal imbalance within the reservoir, which is sufficient to enable the condensation of the vapour on a cooler point of the system, in this case the aluminium sample. Prior to this experiment, the sample is heated to remove any liquid adsorbed on the wall and the wavelength of the SPR corresponding to this state is measured. Then, the surface of the reservoir is heated and the SPR is recorded over time. The results of the experiment are presented in Figure 14 for a temperature of the reservoir close to the ambient, i.e. 25 °C.

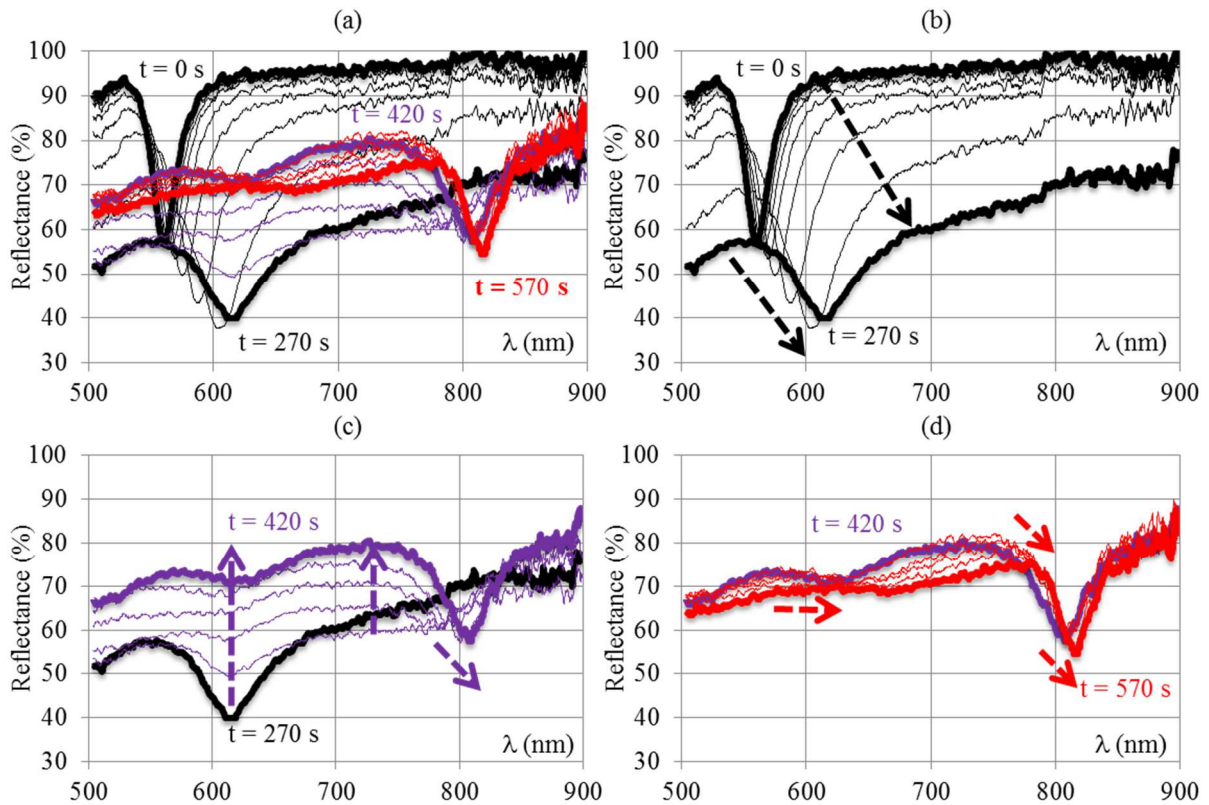


Figure 14: SPR wavelength for an aluminium/acetone interface $\theta_a = 15^\circ$

Figure 14 (a) presents the reflection at an angle $\theta_a = 15^\circ$ of the TM polarized white light measured over the entire visible spectrum at different times varying from $t = 0$ s to $t = 570$ s. For ease of visualization, the results are spread over three different time periods in Figure 14 (b) to Figure 14 (d). At time $t = 0$ s, the SPR is similar to the signal obtained when the aluminium is heated and therefore in contact with vapour only. The wavelength at the SPR is equal to 550 nm. A time $t = 570$ s, the signal does not vary anymore and the surface is covered with a thin

liquid film visible to the naked eye. In these conditions the wavelength at the SPR is equal to 810 nm and is due to the refractive index of the liquid.

From time $t = 0$ s to $t = 270$ s, SPR wavelength increases from 550 nm to about 610 nm showing the change of the refractive index due to the presence of condensation nuclei. Then, from time $t = 270$ s to $t = 420$ s, the intensity of the absorption decreases for $\lambda_{\text{SPR}} = 610$ nm, while at the same time a new SPR wavelength appears for $\lambda_{\text{SPR}} = 800$ nm with an increasing intensity of absorption with time at this wavelength. From time $t = 420$ s to $t = 570$ s, the absorption intensity increases slightly while λ_{SPR} moves from 800 nm to 810 nm. These results are difficult to interpret; the diameter of the light beam incident on the grating is of the order of 3 mm, which means that the measurement area is large compared to the size of the gratings. Thus, the reflected signal incorporates information about a very large area. Nonetheless, the preliminary results clearly show the interest of SPR for the detection of the birth of the nuclei of condensation on the wall, which is not possible with a classical optical method.

The experimental set-up used for the evaporation tests is the same as for the condensation. The reservoir is filled with a small amount of liquid. The procedure consists of covering the surface of the sample with a film of liquid by tilting the chamber horizontally and then tilting the surface vertically again. The liquid initially on the surface flows by gravity and, due to its high wettability on metals, a thin film of liquid adheres to the surface. Immediately after the wetting procedure the absorption peak shifts to about 800 nm (liquid state). The response remains stable, even after an hour's waiting time, because a very thin liquid film adheres to the wall. To evaporate this liquid film, it is necessary to heat the sample using the heating resistor with a heat flux of 10 W.cm^{-2} . Then, the evolution of the plasmonic signal is similar to that obtained for condensation with the same intermediate steps but in the opposite direction.

5. CONCLUSIONS

In this paper, boiling, condensation and evaporation experiments were performed with aluminium samples and acetone as the working fluid. In addition to the thermal analysis of the results obtained with the different samples, experiments using an SPR sensor were carried out to analyse the phenomena taking place at the interface between the metal and the fluid at the nanoscale.

The first part of the article compares boiling curves obtained with different surface finishes, namely unpolished, ultra-smooth, ultra-smooth with 10 unintended defects, ultra-smooth with 24 evenly distributed holes, and a grating coating. The new experimental results obtained with controlled holes realized on a mirror polished surface confirm the conclusions of Al Masri et al. [2], namely that ultra-smooth surfaces with a small number of imperfections deliver the best thermal performance. Furthermore, a critical heat flux of 38 W.cm^{-2} was reached and measured with this surface. Surprisingly, the results obtained with the surface covered with a grating are very similar to the surface with the holes. Further investigations are needed to improve the understanding of these results, for example by increasing the number and the characteristic length of the holes and by changing the depth and the period of the gratings.

The plasmonic method using a periodic corrugated surface was used to study different phase change phenomena. SPR measurements were applied to an experiment of pool boiling during the natural convection phase of the increasing heat flux. The SPR technique enabled a very local measurement of the surface temperature in a non-intrusive way, following a calibration process in a dedicated two-phase experimental rig. Apart from the deviation of the SPR

wavelength due to the wall temperature increase, the experimental results show no modifications of the refractive index of the fluid prior to the onset on nucleate boiling. However, the time resolution of the spectrometer - of the order of 1 ms - is not able to record the very fast incipience process of the bubble 1 ms before the ONB. Furthermore, the SPR method on a corrugated surface cannot be used to analyse the fluid/metal interface state during nucleate boiling, because the incident light is reflected by the bubbles. It might be interesting to test SPR technique based on the attenuated total reflection method in a prism-based structure in these conditions, in which the incident and reflected light would not be disturbed by the presence of macroscopic bubbles on the surface.

In order to evaluate the ability of the method to detect a change in the state of the fluid close to the grating in phase change conditions, condensation and evaporation experiments, which characteristic times are higher than those of nucleate boiling were performed. The plasmonic detection method (SPR) was used to monitor in real time the formation of a nanoscale condensation film and the evaporation of an acetone film. In both cases, a large plasmonic response shift was recorded, showing the liquid/vapour state change. This experiment demonstrated the ability of the SPR method to detect the change in local media index at the nanoscale. It is now necessary to deepen the analysis of the first experimental results to obtained more quantitative results. This requires to calibrate the response of the sensors for different film thickness.

This technique could be extended to the detection of the first frost seeds on a wall and to the characterisation of surfaces that repel or promote condensation or icing. It could also be used to study films adsorbed on a surface.

ACKNOWLEDGEMENTS

The support from the French National Research Agency (ANR) within the ‘‘NUCLEI’’ project (ANR-12-SEED-0003) is gratefully acknowledged.

REFERENCES

- [1] Attinger, D., Frankiewicz, C., Betz, A., Schutzius, T., Ganguly, R., Das, A., . . . Megaridis, C. (2014). Surface engineering for phase change heat transfer: A review. *MRS Energy & Sustainability*, 1, E4. doi:10.1557/mre.2014.9
- [2] Al Masri, M., Cioulachtjian, S., Veillas, C., Verrier, I., Jourlin, Y., Ibrahim, J., ... & Lefevre, F. (2017). Nucleate boiling on ultra-smooth surfaces: Explosive incipience and homogeneous density of nucleation sites. *Experimental Thermal and Fluid Science*, 88, 24-36. doi.org/10.1016/j.expthermflusci.2017.05.008.
- [3] Meyer, J., & De Paepe, M. (Eds.). (2020). *The Art of Measuring in the Thermal Sciences* (1st ed.). CRC Press. <https://doi.org/10.1201/9780429201622>
- [4] Narayan, L. S., & Srivastava, A. (2021). Non-contact experiments to quantify the microlayer evaporation heat transfer coefficient during isolated nucleate boiling regime. *International Communications in Heat and Mass Transfer*, 122, doi.org/10.1016/ 105191.
- [5] Blander, M., & Katz, J. L. (1975). Bubble nucleation in liquids. *AIChE Journal*, 21(5), 833-848.
- [6] Sheng, Q., Sun, J., Wang, Q., Wang, W., & Wang, H. S. (2016). On the onset of surface condensation: formation and transition mechanisms of condensation mode. *Scientific reports*, 6(1), 1-9.
- [7] Cox, S. J., Kathmann, S. M., Slater, B., & Michaelides, A. (2015). Molecular simulations of heterogeneous ice nucleation. I. Controlling ice nucleation through surface hydrophilicity. *The Journal of chemical physics*, 142(18), 184704.

- [8] Gatapova, E. Y., Graur, I. A., Kabov, O. A., Aniskin, V. M., Filipenko, M. A., Sharipov, F., & Tadrist, L. (2017). The temperature jump at water–air interface during evaporation. *International Journal of Heat and Mass Transfer*, 104, 800-812.
- [9] Kim, H., & Buongiorno, J. (2011). Detection of liquid–vapor–solid triple contact line in two-phase heat transfer phenomena using high-speed infrared thermometry. *International Journal of Multiphase Flow*, 37(2), 166-172.
- [10] BARNES, W. L., DEREUX, A., EBBESEN, T.W., 2003, Surface plasmon subwavelength optics. *nature*, vol. 424, no 6950, 824-830. doi:10.1038/nature01937
- [11] Homola, J., 2006. *Surface plasmon resonance-based sensors*. Springer.
- [12] Sommerfeld, A., 1899. Über die Fortpflanzung elektrodynamischer Wellen längs eines Drahtes. *Ann. Phys.* 303, 233–290. doi:10.1002/andp.18993030202
- [13] Zenneck, J., 1907. Über die Fortpflanzung ebener elektromagnetischer Wellen längs einer ebenen Leiterfläche und ihre Beziehung zur drahtlosen Telegraphie. *Ann. Phys.* 328, 846–866. doi:10.1002/andp.19073281003
- [14] Wood, R. w., 1902. XLIV. A suspected case of the electrical resonance of minute metal particles for light-waves. A new type of absorption. *Philosophical Magazine Series 6* 3, 396–410. doi:10.1080/14786440209462780
- [15] Pockrand, I., Swalen, J.D., 1978. Anomalous dispersion of surface plasma oscillations. *J. Opt. Soc. Am., JOSA* 68, 1147–1151. doi:10.1364/JOSA.68.001147
- [16] Fleischmann, M., Hendra, P.J., McQuillan, A.J., 1974. Raman spectra of pyridine adsorbed at a silver electrode. *Chemical Physics Letters* 26, 163–166. doi:10.1016/0009-2614(74)85388-1
- [17] Nylander, C., Liedberg, B., Lind, T., 1982. Gas detection by means of surface plasmon resonance. *Sensors and Actuators* 3, 79–88. doi:10.1016/0250-6874(82)80008-5
- [18] Liedberg, B., Nylander, C., Lunström, I., 1983. Surface plasmon resonance for gas detection and biosensing. *Sensors and Actuators* 4, 299–304. doi:10.1016/0250-6874(83)85036-7
- [19] Homola, J., 2003. Present and future of surface plasmon resonance biosensors. *Anal Bioanal Chem* 377, 528–539. doi:10.1007/s00216-003-2101-0
- [20] Lakowicz, J.R., 2006. *Plasmonics in Biology and Plasmon-Controlled Fluorescence*. *Plasmonics* 1, 5–33. doi:10.1007/s11468-005-9002-3
- [21] Masson, J-F., Murray-Méthot, M.-P., Live, L.S., 2010. Nanohole arrays in chemical analysis: manufacturing methods and applications. *Analyst* 135, 1483–1489. doi:10.1039/C0AN00053A
- [22] Ferry, V.E., Verschuuren, M.A., Li, H.B.T., Verhagen, E., Walters, R.J., Schropp, R.E.I., Atwater, H.A., Polman, A., 2010. Light trapping in ultrathin plasmonic solar cells. *Opt. Express*, OE 18, A237–A245. doi:10.1364/OE.18.00A237
- [23] Atwater, H.A., Polman, A., 2010. Plasmonics for improved photovoltaic devices. *Nat Mater* 9, 205–213. doi:10.1038/nmat2629
- [24] Lethiec, C., 2014. *Emission polarisée de nanoémetteurs : excitation de plasmons sur une surface métallique* (phdthesis). Université Pierre et Marie Curie - Paris VI.
- [25] Berini, P., 2000. Plasmon polariton waves guided by thin lossy metal films of finite width: bound modes of symmetric structures. *Phys. Rev. B*, 61 (15), 10484-10503.
- [26] Sauvage-Vincent, J., Tonchev, S., Veillas, C., Reynaud, S., & Jourlin, Y. (2013). Optical security device for document protection using plasmon resonant transmission through a thin corrugated metallic film embedded in a plastic foil. *Journal of the European Optical Society-Rapid publications*, 8, 13015. doi: :10.2971/jeos.2013.13015
- [27] Holmgaard, T., Chen, Z., Bozhevolnyi, S.I., Markey, L., Dereux, A., Krasavin, A.V., Zayats, A.V., 2009. Wavelength selection by dielectric-loaded plasmonic components. *Appl. Phys. Lett.* 94, 051111. doi:10.1063/1.3078235
- [28] Bachelot, R., Gleyzes P., Boccara, A.C., 1995. Near-field optical microscope based on local perturbation of a diffraction spot, *Opt. Lett.* 20, 1924.
- [29] Jeong, C. H., Lee, S. H., Shin, D. H., Konduru, V., Allen, J. S., & Choi, C. K. (2017). High speed SPR visualization of frost propagation inside a subcooled water droplet. *Journal of Heat Transfer*, 139(2).

- [30] Jeong, C. H., Shin, D. H., Konduru, V., Allen, J. S., Choi, C. K., & Lee, S. H. (2018). Quantitative measurements of nanoscale thin frost layers using surface plasmon resonance imaging. *International Journal of Heat and Mass Transfer*, 124, 83-89.
- [31] Ibrahim, J., Al Masri, M., Veillas, C., Celle, F., Cioulachtjian, S., Verrier, I., Lefèvre, F, Jourlin, Y. (2017). Condensation phenomenon detection through surface plasmon resonance. *Optics express*, 25(20), 24189-24198.
- [32] Ibrahim, J., Al Masri, M., Verrier, I., Kampfe, T., Veillas, C., Celle, F., Lefèvre, F., Jourlin, Y. (2019). Surface plasmon resonance-based temperature sensors in liquid environment. *Sensors*, 19(15), 3354.
- [33] Kim, D. Y., Jeong, C. H., Lee, H. J., Choi, C. K., & Lee, S. H. (2020). Modeling of the finite boundary limit of evaporation flux in the contact line region using the surface plasmon resonance imaging. *International Communications in Heat and Mass Transfer*, 116, 104598.
- [34] Freestone, I., Meeks, N., Sax, M., Higgitt, C., 2007. The Lycurgus cup—a roman nanotechnology. *Gold bulletin*, vol. 40, no 4, p. 270-277.
- [35] Homola, J., Koudela, I., & Yee, S. S. (1999). Surface plasmon resonance sensors based on diffraction gratings and prism couplers: sensitivity comparison. *Sensors and Actuators B: Chemical*, 54(1-2), 16-24.
- [36] Rheims, J., Köser, J., & Wriedt, T. (1997). Refractive-index measurements in the near-IR using an Abbe refractometer. *Measurement Science and Technology*, 8(6), 601.
- [37] Kim, Y. H., Park, S. J., Jeon, S. W., Ju, S., Park, C. S., Han, W. T., & Lee, B. H. (2012). Thermo-optic coefficient measurement of liquids based on simultaneous temperature and refractive index sensing capability of a two-mode fiber interferometric probe. *Optics express*, 20(21), 23744-23754.